

# Topological Data Analysis of COVID-19 Virus Spike Proteins

Moo K. Chung<sup>1</sup> and Hernando Ombao<sup>2</sup>

<sup>1</sup>University of Wisconsin, Madison, USA

<sup>2</sup>King Abdullah University of Science and Technology, Thuwal, Saudi Arabia

mkchung@wisc.edu, hernando.ombao@kaust.edu.sa

**Abstract.** Topological data analysis, including persistent homology, has undergone significant development in recent years. However, due to heterogeneous nature of persistent homology features that do not have one-to-one correspondence across measurements, it is still difficult to build a coherent statistical inference procedure. The paired data structure in persistent homology as birth and death events of topological features add further complexity to conducting inference. To address these current problems, we propose to analyze the birth and death events using lattice paths. The proposed lattice path method is implemented to characterize the topological features of the protein structures of corona viruses. This demonstrates new insights to building a coherent statistical inference procedure in persistent homology.

## 1 Introduction

Topological data analysis (TDA) was introduced 20 years ago. Despite its rigorous mathematical foundation, it still suffers from numerous statistical and computational problems (Edelsbrunner et al. 2000). Due to these practical issues, TDA has not yet become a standard tool for scientists. Persistent homology has been applied to wide variety of biomedical data including brain networks (Chung, Lee, DiChristofano, Ombao & Solo 2019), protein structures (Gameiro et al. 2015) and RNA viruses (Chan et al. 2013). Yet, most of these methods only serve as exploratory tools that provide descriptive summary statistics. The main difficulty is due to the heterogeneous nature of topological features which do not have one-to-one correspondence across measurements. For instance, Figure 1-top displays often used persistent diagrams that may have different number of scatter points that do not have one-to-one correspondence across the different persistent diagrams. This lack of proper matching has been one of the obstacles to building a coherent statistical analysis directly on the scatter points. In Garside et al. (2020), the birth and death of  $k$ -cycles are modeled as the “observed data” in the event history analysis in a literal sense. The entire event is collapsed by accumulating the persistences and then transformed into a single summary measure for statistical analysis across subjects.

Motivated by these statistical challenges, we propose a more principled approach to developing a statistical inference procedure through the order statistics and combinatorial enumeration through lattice paths. The proposed *topological lattice path* method

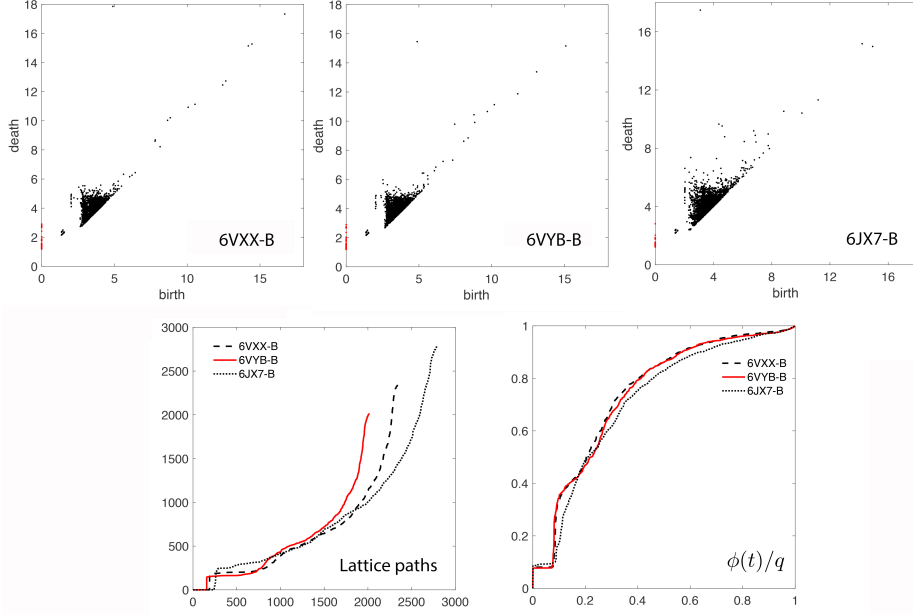


**Fig. 1.** Top: persistent diagrams of three different spike proteins. The red dots are 0-cycles and the black dots are 1-cycles. The units are in Å (angstrom). Bottom: corresponding lattice paths and normalized step functions  $\phi(t)/q$ .

demonstrated to differentiating the conformational changes of the COVID-19 virus spike proteins that is crucial in vaccine development (Walls et al. 2020, Cai et al. 2020).

## 2 Simplicial homology for protein structures

A high dimensional object (e.g., proteins) can be modeled using point cloud data  $V$  consisting of  $p$  number of points (atoms) indexed as  $V = \{1, 2, \dots, p\}$ . Suppose the distance  $\rho_{ij}$  between points  $i$  and  $j$  satisfies the metric properties. For proteins, we can simply use the Euclidean distance between atoms in a molecule. Then  $\mathcal{X} = (V, \rho)$ ,  $\rho = (\rho_{ij})$  is a metric space where we can build a filtration necessary for persistent homology. If we connect points following some criterion on the distance, they will form a simplicial complex which will follow the topological structure of the molecule (Edelsbrunner & Harer 2010, Hart 1999, Zomorodian 2009). Note that the  $k$ -simplex is the convex hull of  $k + 1$  points in  $V$ . A simplicial complex is a finite collection of simplices such as points (0-simplex), lines (1-simplex), triangles (2-simplex) and higher dimensional counterparts. In particular, the *Rips complex*  $\mathcal{X}_\epsilon$  is a simplicial complex, whose  $k$ -simplices are formed by  $(k + 1)$  points which are pairwise within distance  $\epsilon$  (Ghrist 2008). While a graph has at most 1-simplices, the Rips complex has at most  $(p - 1)$ -simplices. The Rips complex induces a hierarchical nesting structure called the Rips filtration

$$\mathcal{X}_{\epsilon_0} \subset \mathcal{X}_{\epsilon_1} \subset \mathcal{X}_{\epsilon_2} \subset \dots$$

for  $0 = \epsilon_0 < \epsilon_1 < \epsilon_2 < \dots$ , where the sequence of  $\epsilon$ -values are called the filtration values. The filtration is quantified through a topological basis called *k-cycles*. 0-cycles are the connected components, 1-cycles are 1D closed path or loop while 2-cycles are a 2-simplices without interior. Any *k-cycles* can be represented as a linear combination of basis *k-cycles*. The Betti numbers  $\beta_k$  counts the number of independent *k-cycles*. During the Rips filtration, the *i*-th *k-cycles* are born at filtration value  $b_i$  and die at  $d_i$ . The collection of all the paired filtration values  $\{(b_1, d_1), \dots, (b_q, d_q)\}$  displayed as 1D intervals is called the *barcode* and displayed as scatter points in 2D plane is called the *persistent diagram*. Since  $b_i < d_i$ , the scatter points in the persistent diagram are traditionally displayed above the line  $y = x$  line by taking births in the *x*-axis and deaths in the *y*-axis. Figure 1-top displays the persistent diagrams of three different spike proteins used in the study.

### 3 Barcodes as lattice paths

The first step in the *topological lattice path method* is to sort all the birth and death values in the filtration as an order statistic

$$c : c_1 < c_2 < \dots < c_{2q},$$

where  $c_i$  is one of birth or death values. We will simply call such sequence as the *birth-death process*. During the filtration, the sequence of birth and death occurs somewhat randomly but still with specific pairing structure that is equivalent to having balanced brackets. If we denote births by the left bracket “[” and deaths by the right bracket “]”, some sequences are valid and while some are not. For instance, the following sequences of size  $l = 3$  are valid:

$$[[[]]], [[]][], [[[]]]$$

while the following sequences are not valid

$$][[]], [[]][[], [[[]][$$

since the bold brackets are not properly paired. Thus, every possible valid sequence of birth and death values can be viewed as forming a probability space, where each valid sequence is likely to happen with equal probability. The total number of such valid sequences is called the Catalan number  $\kappa_p$  (Simion 2000) given by

$$\kappa_p = \frac{1}{q+1} \binom{2q}{q}.$$

The first few Catalan numbers are  $\kappa_1 = 1, \kappa_2 = 2, \kappa_3 = 5, \kappa_4 = 14$ . The Catalan number increases exponentially. Using Stirling’s formula we can show that (Chung, Xie, Huang, Wang, Yan & Shen 2019)

$$\kappa_q \sim \frac{4^q}{\sqrt{\pi q}(q+1)}.$$

The number of possible filtrations *exponentially* increases as the number of birth and death values increases. Many computational algorithms associated with the birth-death

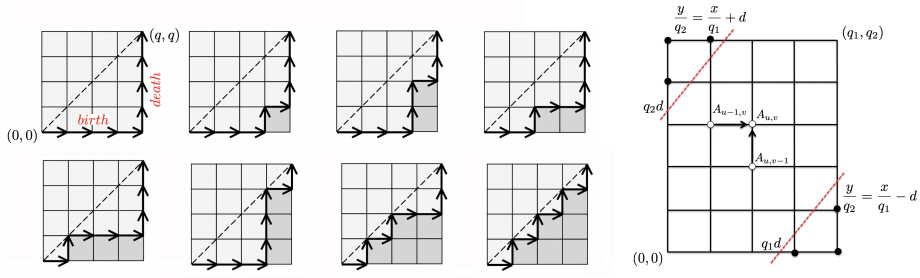


**Fig. 2.** Left: the lattice path representation of processes with  $q$  birth and  $q$  death events. Right: The problem of testing the topological equivalence of birth-death processes of lengths  $q_1$  and  $q_2$  can be transformed to a problem of lattice path enumeration between 0 and  $(q_1, q_2)$  with the constraint  $|x/q_1 - y/q_2| < d$ .

processes are costly and slow to converge. One of our goals here to provide a remedy to this problem.

The Catalan number is also related to the number of possible *non-crossing* partitions, which enumerates the number of possible hierarchical clusterings with  $q$  elements or the number of binary trees out of  $q$  leaf nodes (Billera et al. 2001, Simion 2000). The Catalan number is also the total number of monotone *lattice paths* between  $(0, 0)$  and  $(q, q)$  in  $\mathbb{Z}^2$  with horizontal step  $\rightarrow$  or vertical step  $\uparrow$  but with a constrain that they do not pass above the diagonal line  $y = x$  (Stanley 1999). Figure 2-left displays 8 valid lattice paths out of 14 possibilities for  $q = 4$ . There exists one-to-one relation between the ordered sequence of birth and death events and a lattice path if we identify births with  $\rightarrow$  and deaths with  $\uparrow$ . The path above  $y = x$  is not valid since it is not possible to have more deaths than births. Moreover, rapid changes in the direction of paths implies more fleeting fluctuations that may be viewed as topological noise. The first path in Figure 2 has larger persistence while the last path has smaller persistence. We can further transform lattice paths to unique monotone functions.

**Theorem 1.** *There exists a one-to-one map from the valid ordering in a birth-death process to a strictly increasing step function  $\phi$  with range 0 to  $q$ .*

We explicitly construct such function  $\phi$ . Consider the heights of boxes below lattice paths (dark gray colored boxes in Figure 2) as we traverse the path. Denote the sequence of heights as

$$h : h_1 \leq h_2 \leq \dots \leq h_q.$$

This sequence is monotonically non-decreasing. In Figure 2, the height of boxes in the first path is represented as  $(0, 0, 0, 0)$  while the last path is represented as  $(0, 1, 2, 3)$ . The total number of boxes below the path is related to persistence. A barcode with smaller persistences (last path in Figure 2) will have a greater number of boxes while longer persistences will not have many boxes (first path in Figure 2). Given the sequence of heights, the corresponding lattice path can be recovered by tracing the outline of boxes. Consequently, the order of pairing is also recovered.

If births occur  $r$  times sequentially in the birth-death process, the sequence of heights  $h$  will have  $r$  repeated subsequences. To ensure that the sequence  $h$  strictly increasing, we simply add  $(0, \frac{1}{r}, \frac{2}{r}, \dots, \frac{r-1}{r})$  to the repetition.

For instance, the first path  $(0, 0, 0, 0)$  in Figure 2 can be made strictly monotone by adding  $(0, \frac{1}{4}, \frac{2}{4}, \frac{3}{4})$ . We now construct  $\phi(t)$  as a step function where jumps occur at each element of  $h$ :

$$\phi(t) = \begin{cases} 0 & \text{if } t \in [0, \frac{h_1}{q}) \\ j & \text{if } t \in [\frac{h_j}{q}, \frac{h_{j+1}}{q}) \text{ for } j = 1, \dots, q-1 \\ q & \text{if } t \in [\frac{h_q}{q}, 1] \end{cases} .$$

The normalized step function  $\phi(t)/q$  can be viewed as an *empirical cumulative distribution* and many statistical tools on distributions can be immediately applicable without any harm. From  $\phi(t)$ , the original sequence  $h$  and the ordering in the birth-death process can be both recovered. Thus, the map is invertible and one-to-one. Figure 1-bottom displays the lattices paths and the normalized step functions of 1-cycles corresponding to the spike proteins used in the study. The proposed *topological lattice path* method uses  $\phi(t)/q$  as a new topological functional descriptor over persistent diagrams or barcodes and this is the main novelty of the study.

#### 4 Exact topological inference for birth-death process

The task is to develop a method for testing the *equivalence* of two monotone functions from persistent diagrams or barcodes. This will be conducted by testing the equivalence of two independently observed birth-death processes:

$$\begin{aligned} C^1 &: c_1^1 < c_2^1 < \dots < c_{q_1}^1 \\ C^2 &: c_1^2 < c_2^2 < \dots < c_{q_2}^2, \end{aligned}$$

where each element is either birth or death and  $q_1$  and  $q_2$  are the numbers of pairings. Following Theorem 1, we construct two strictly monotone functions  $\phi_1$  and  $\phi_2$  corresponding to  $C^1$  and  $C^2$ . The topological distance

$$D(\phi_1, \phi_2) = \sup_t \left| \frac{\phi_1(t)}{q_1} - \frac{\phi_2(t)}{q_2} \right|,$$

will be used as the test statistic for testing the equivalence of  $C^1$  and  $C^2$ . The scaling by the denominators  $q_1$  and  $q_2$  ensure that the value of step functions is in  $[0, 1]$ . The distance is motivated by the Kolmogorov-Smirnov (KS) test statistic (Böhm & Hornik 2010, Gibbons & Chakraborti 2011, Chung et al. 2017).

**Theorem 2.** *Under the null hypothesis of the equivalence of  $C^1$  and  $C^2$ ,*

$$P(D(\phi^1, \phi^2) \geq d) = 1 - \frac{A_{q_1, q_2}}{\binom{q_1 + q_2}{q_1}},$$

where  $A_{u,v}$  satisfies  $A_{u,v} = A_{u-1,v} + A_{u,v-1}$  with the boundary condition  $A_{q_1, 0} = A_{0, q_2} = 1$  within the band  $|u/q_1 - v/q_2| < d$ .

The statement can be proved similarly as the combinatorial construction of KS-test that also uses the lattice path enumeration (Böhm & Hornik 2010, Gibbons & Chakraborti 2011, Chung et al. 2017). Combine monotonically increasing sequences  $C^1$  and  $C^2$  and sort them into a bigger monotone sequence of size  $q_1 + q_2$ . Represent the integrated sequence as the sequence of  $\rightarrow$  and  $\uparrow$  respectively depending on if they are coming from  $C^1$  or  $C^2$ . Under the null, there is no preference and they come equally likely from  $C^1$  or  $C^2$ . If we follows the sequence of arrows, it forms a monotone lattice path from  $(0, 0)$  to  $(q_1, q_2)$ . There are total  $\binom{q_1+q_2}{q_1}$  possible equally likely lattice paths that forms the sample space. This is equivalent to the total number of permutations in a two-sample test.

From Theorem 1, the values of  $\phi_1(t)$  and  $\phi_2(t)$  are integers from 0 to  $q$ . Thus,  $(\phi_1(t), \phi_2(t))$  are the  $(x, y)$ -coordinates in lattice paths. Note  $\sup_t |\phi_1(t)/q_1 - \phi_2(t)/q_2| < d$  if and only if  $|\phi_1(t)/q_1 - \phi_2(t)/q_2| < d$  for all  $t$ . Such points are all the lattice points satisfying within the band bounded by two lines  $y/q_2 = x/q_1 \pm d$  (dotted red lines in Figure 2). Thus the probability of event  $D < d$  is the number of valid paths over the every possible paths given by

$$P(D \geq d) = 1 - P(D_q < d) = 1 - \frac{A_{q_1, q_2}}{\binom{q_1+q_2}{q_1}}, \quad (1)$$

where  $A_{u,v}$  be the total number of valid paths from  $(0, 0)$  to  $(u, v)$ . Since there is only two paths leading to  $(u, v)$ , it can be written as

$$A_{u,v} = A_{u-1,v} + A_{u,v-1}.$$

If there is no constraint,  $A_{u,v} = \binom{u+v}{u}$  but due to the constraint, it has to be iteratively computed with the boundary condition  $A_{u,0} = A_{0,v} = 1$  for all  $u$  and  $v$ . We start from the bottom left corner  $(0, 0)$  and move toward the top right corner  $(q_1, q_2)$  in solving the recursion numerically:

$$A_{0,0} = 0 \rightarrow A_{1,0} = A_{0,1} = 1, A_{1,1} = 2 \rightarrow A_{2,0} = 0, \dots \rightarrow A_{q_1, q_2} = A_{q_1-1, q_2} + A_{q_1, q_2-1}.$$

Computing  $A_{q_1, q_2}$  iteratively requires at most  $q_1 \cdot q_2$  operations while the permutation test will cause a computational bottleneck for large  $q_1$  and  $q_2$  (Chung, Xie, Huang, Wang, Yan & Shen 2019). The *topological lattice path* method computes the exact  $p$ -value substantially faster than the permutation test.

Most protein molecules consist of thousands of atoms and hence number of pairings  $q_1$  and  $q_2$  should be sufficient for the asymptotic approximation below:

**Theorem 3.**  $\lim_{q_1, q_2 \rightarrow \infty} P\left(\sqrt{\frac{q_1 q_2}{q_1 + q_2}} D \geq d\right) = 2 \sum_{j=1}^{\infty} (-1)^{j-1} e^{-2j^2 d^2}.$

The result follows by treating  $\phi_1/q_1$  and  $\phi_2/q_2$  as the empirical cumulative distribution functions and using the asymptotic expansion of the KS-test (Gibbons & Chakraborti 2011, Smirnov 1939). Subsequently, the  $p$ -value under null is given by

$$p\text{-value} = 2e^{-d_o^2} - 2e^{-8d_o^2} + 2e^{-18d_o^2} \dots,$$

where  $d_o$  is the observed value of  $\sqrt{\frac{q_1 q_2}{q_1 + q_2}} D$ . For any large observed value  $d_o \geq 2$ , the second term is in the order of  $10^{-14}$  and insignificant. Even for a small value of  $d$

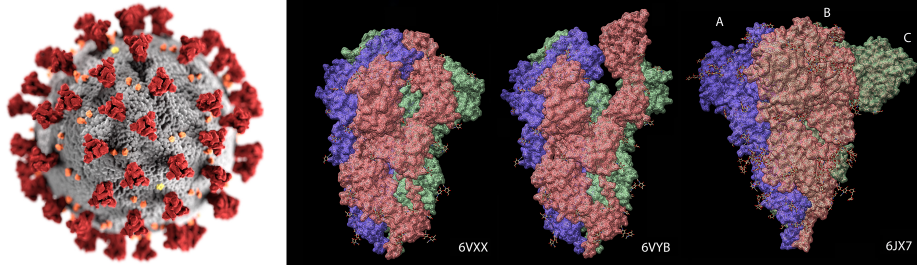


**Fig. 3.** Left: Schematic representation of COVID-19 virus with spike proteins (red). Right: Spike proteins of the three different corona viruses. The spike proteins consist of three similarly shaped intertwining substructures identified as A (blue), B (red) and C (green) domains.

$d_o$ , the expansion converges quickly and 5 terms should be more than sufficient to use Theorem 3.

## 5 Topological analysis of the spike proteins of COVID-19 virus

The *topological lattice path* method is used to study the topological structure of the severe acute respiratory syndrome coronavirus 2 (SARS-Cov-2), which is often called COVID-19. Since the start of the global pandemic (approximately December 2019), COVID-19 has already caused 3 million deaths in the world as of April 2021. The COVID-19 virus is specific member of a much broader coronavirus family, which all have spike proteins surrounding the spherically shaped virus similar to the sun's corona. The glycoprotein spikes that bind with receptors on cells and consequently cause a severe infection. The atomic structure of spike proteins can be determined through the cryogenic electron microscopy (cryo-EM) (Walls et al. 2020, Cai et al. 2020). Figure 3-left illustrates spike proteins (colored red) that surrounds the spherically shaped virus. Each spike consists of three similarly shaped protein molecules with rotational symmetry often identified as A, B and C domains. The spike proteins have two distinct conformations identified as *open* and *closed* states, where the domain's opening is necessary for interfacing with the host cell's surface for membrane fusion and viral entry (Figure 3-right). Indeed, most current vaccine efforts focus on preventing the open state from interfacing with the host cell and thus of prime importance in vaccine development and therapeutics (Cai et al. 2020).

In this study, we analyzed the spike of three different coronaviruses identified as 6VXX, 6VYB (Walls et al. 2020) and 6JX7 (Yang et al. 2020). The 6VXX and 6VYB are the closed and open states of SARS-Cov-2 from human while 6JX7 is feline coronavirus (Figure 3). All the domains of 6VXX have exactly 7604 atoms and are expected to be topologically identical. Following the *topological lattice path* method on 1-cycles, we tested if the B-domain is topologically equivalent to the A- and C-domain within 6VXX. The normalized step functions are almost identical and the observed topological distances are 0.0090 and 0.0936, which give the  $p$ -value of 1.0000. Thus, we conclude that they are topologically equivalent as expected. Figure 1 displays the lattice path and

the normalized step functions for domain B. The plots for other domains are visually almost inseparable and hence not shown.

The closed domain B of 6VXX is also compared against the open domain B of 6VYB. The open state has a significantly reduced number of atoms at 6865 due to the conformation change that may change topology as well. The observed topological distance is 0.2 and the test shows the extremely small  $p$ -values of  $8.1123 \times 10^{-38}$  confirming the topological change. The persistent diagrams of both closed and open states are almost identical in smaller birth and death values below 6 Å (angstrom). The major difference is in scatter points with larger birth and death values (Figure 1). The *topological lattice path* method confirms that the local topological structures are almost identical while the global topological structures are changing.

The domain B of 6VXX is also compared against the domain B of feline coronavirus 6JX7 consisting of 9768 atoms. Since 6JX7 is not from human, it is expected that they are different. The topological distance is 0.9194 and  $p$ -values is 0 confirming different topological nature of spikes. This shows the biggest topological difference among all the comparisons done in this study.

## 6 Conclusions

We presented a new representation of persistent diagrams using lattice paths. The novel representation enables us to perform the statistical inference combinatorially through the proposed *topological lattice path* method by enumerating every possible valid lattice paths analytically. The *topological lattice path* method is subsequently used to analyze the coronavirus spike proteins. The normalized step function  $\phi(t)/q$  for all the spike proteins show fairly stable consistent global monotone pattern but with localized differences. We demonstrated the *topological lattice path* method has the ability to statistically discriminate between the conformation changes of the spike protein that is needed in the transmission of the virus. We hope that the our new representation enables scientists in automatic identification of different types and states of coronaviruses in a more principled manner. Currently this is mainly done manually through visual inspection.

## 7 Acknowledgement

The schematic illustration of COVID-19 virus is provided by Alissa Eckert and Dan Higgins of Disease Control and Prevention (CDC), US. The proteins 6VXX and 6VYB are provided by Alexander Walls of University of Washington. The protein 6JX7 is provided by Tzu-Jing Yang of National Taiwan University. Figure 2-left is modified from an image in Wikipedia. This study is supported by NIH R01 EB022856 and R01 EB028753, NSF MDS-2010778, and CRG from the King Abdullah University of Science and Technology (KAUST).



## Bibliography

- Billera, L., Holmes, S. & Vogtmann, K. (2001), 'Geometry of the space of phylogenetic trees', *Advances in Applied Mathematics* **27**, 733–767.
- Böhm, W. & Hornik, K. (2010), 'A Kolmogorov-Smirnov test for  $r$  samples', *Institute for Statistics and Mathematics Research Report Series*, Report 105.
- Cai, Y., Zhang, J., Xiao, T., Peng, H., Sterling, S., Walsh, R., Rawson, S., Rits-Volloch, S. & Chen, B. (2020), 'Distinct conformational states of SARS-CoV-2 spike protein', *Science* **369**, 1586–1592.
- Chan, J. M., Carlsson, G. & Rabadan, R. (2013), 'Topology of viral evolution', *Proceedings of the National Academy of Sciences* **110**(46), 18566–18571.
- Chung, M., Lee, H., DiChristofano, A., Ombao, H. & Solo, V. (2019), 'Exact topological inference of the resting-state brain networks in twins', *Network Neuroscience* **3**, 674–694.
- Chung, M., Vilalta-Gil, V., Lee, H., Rathouz, P., Lahey, B. & Zald, D. (2017), 'Exact topological inference for paired brain networks via persistent homology', *Information Processing in Medical Imaging (IPMI), Lecture Notes in Computer Science (LNCS)* **10265**, 299–310.
- Chung, M., Xie, L., Huang, S.-G., Wang, Y., Yan, J. & Shen, L. (2019), Rapid acceleration of the permutation test via transpositions, in 'International Workshop on Connectomics in Neuroimaging', Vol. 11848, Springer, pp. 42–53.
- Edelsbrunner, H. & Harer, J. (2010), *Computational topology: An introduction*, American Mathematical Society.
- Edelsbrunner, H., Letscher, D. & Zomorodian, A. (2000), Topological persistence and simplification, in 'Foundations of Computer Science, 2000. Proceedings. 41st Annual Symposium on', IEEE, pp. 454–463.
- Gameiro, M., Hiraoka, Y., Izumi, S., Kramar, M., Mischaikow, K. & Nanda, V. (2015), 'A topological measurement of protein compressibility', *Japan Journal of Industrial and Applied Mathematics* **32**, 1–17.
- Garside, K., Gjoka, A., Henderson, R., Johnson, H. & Makarenko, I. (2020), 'Event history and topological data analysis', *arXiv preprint arXiv:2012.08810*.
- Ghrist, R. (2008), 'Barcodes: The persistent topology of data', *Bulletin of the American Mathematical Society* **45**, 61–75.
- Gibbons, J. D. & Chakraborti, S. (2011), *Nonparametric Statistical Inference*, Chapman & Hall/CRC Press.
- Hart, J. (1999), Computational topology for shape modeling, in 'Proceedings of the International Conference on Shape Modeling and Applications', pp. 36–43.
- Simion, R. (2000), 'Noncrossing partitions', *Discrete Mathematics* **217**(1-3), 367–409.
- Smirnov, N. (1939), 'Estimate of deviation between empirical distribution functions in two independent samples', *Bulletin of Moscow University* **2**, 3–16.
- Stanley, R. (1999), *Enumerative combinatorics. Vol. 2*, Cambridge Studies in Advanced Mathematics.
- Walls, A., Park, Y.-J., Tortorici, M., Wall, A., McGuire, A. & Veesler, D. (2020), 'Structure, function, and antigenicity of the SARS-CoV-2 spike glycoprotein', *Cell* **181**, 281–292.

- Yang, T.-J., Chang, Y.-C., Ko, T.-P., Draczkowski, P., Chien, Y.-C., Chang, Y.-C., Wu, K.-P., Khoo, K.-H., Chang, H.-W. & Hsu, S.-T. D. (2020), 'Cryo-EM analysis of a feline coronavirus spike protein reveals a unique structure and camouflaging glycans', *Proceedings of the National Academy of Sciences* **117**, 1438–1446.
- Zomorodian, A. (2009), *Topology for computing*, Vol. 16 of *Cambridge Monographs on Applied and Computational Mathematics*, Cambridge University Press, Cambridge.